

Investigating a new neutral heavy gauge boson within the mono- Z' portal via simulated pp collisions at $\sqrt{s} = 14$ TeV at the HL-LHC.

Ali Muhammad H. H.*

*Physics Department, Faculty of Science, Ain Shams University, Cairo,
Basic Science Department, Faculty of Engineering, The British University in Egypt, Cairo*

El-sayed A. El-dahshan

Physics Department, Faculty of Science, Ain Shams University, Cairo

S. Elgammal

*Centre for Theoretical Physics, The British University in Egypt,
P.O. Box 43, El Sherouk City, Cairo 11837, Egypt.*

In this study, we aim to explore the potential for generating events related to dark matter (DM) in conjunction with a neutral heavy gauge boson (Z') decaying leptonically during proton-proton collisions at the Large Hadron Collider (LHC). These collisions occur at a center-of-mass energy of $\sqrt{s} = 14$ TeV, with a high integrated luminosity equivalent to 1000 fb^{-1} . Our analysis involves interpreting the outcomes through Monte Carlo simulation of the effective field theory (EFT) framework. If no new physics is detected, we establish constraints on various parameters within the EFT context, such as the scenario cutoff scale (Λ) and the Z' mass.

Keywords: The High-Luminosity Large Hadron Collider HL-LHC, Large Hadron Collider LHC, New neutral heavy gauge boson, The Compact Muon Solenoid CMS, Dark matter

I. INTRODUCTION

There is a strong belief in scientific circles, based on astronomical observations, that the known baryonic matter is not the whole story and only forms about 27% of the universe's mass [1–9]. The rest is attributed to dark energy and dark matter (DM). This mystery of DM has been an ongoing research point for astronomers and particle physicists on equal feet for decades. Trying to solve this mystery is one of the main purposes of the CERN Large Hadron Collider's (LHC) most famous experiments, CMS and ATLAS.

The most prosperous theory in particle physics is the standard model of particle physics (SM), in which two of the four fundamental forces, electromagnetism, and the weak nuclear force, are unified in one entity called the electroweak force [10]. Although this theory has accomplished great success, the last of them was the discovery of the Higgs boson at the LHC in 2012 by ATLAS and CMS collaborations [11], it fails to answer a wide range of questions of interest, including what particles form DM [10, 12].

Many theorists have proposed various theories beyond the standard model (BSM) hoping to extend the success of the SM to more than discovering the Higgs particle and being obsessed with finding the DM particles [12]. Some of the promising BSM models have a topology, referred to as "mono-X", and make predictions about possible occurrences involving the production of DM in association with a visible particle, Which acts as a candle, single photon, quark, or gauge boson (i.e. Z, W or Higgs) [13–18].

These occurrences are identified by visible state particles and a substantial amount of missing transverse energy (E_T^{miss}) signifying the presence of DM.

In alternative models, X might be an unseen particle, such as the heavy neutral gauge boson Z' . One example of DM models is proposed in [19] with topology mono- Z' , in which DM particles can be generated alongside Z' through three potential scenarios: the light vector (LV), dark Higgs (DH), and effective field theory (EFT). This model is sensitive at 14 TeV LHC as proposed in [20]. Both the CMS and ATLAS collaborations have previously searched for the massive extra neutral gauge boson, Z' , which is a prediction of Grand Unified Theory (GUT) and Supersymmetry [21–24]. Despite their efforts, they found no evidence for its existence using the complete RUN II dataset from the LHC up to 5.2 TeV of the dilepton invariant mass [25, 26].

In addition, the ATLAS collaboration has investigated the leptonic decay of Z' [27] and its hadronic decay [28] produced in association with dark matter. They thoroughly examined the LV and DH scenarios. Neither the CMS nor ATLAS collaboration has explored the EFT interpretation of the mono- Z' portal. In reference [27], they used the full run-2 data taken by the LHC at 13 TeV center-of-mass energy (\sqrt{s}) of proton-proton collisions with an integrated luminosity of 140 fb^{-1} . This search has ruled out Z' masses ranging from 200 to 450 GeV for the heavy dark sector of the LV scenario, taking $g_q = g_l = 0.1$ and $g_D = 1.0$, where g_q , g_l , and g_D are the couplings of the Z' to the SM quarks, leptons, and DM particles, respectively.

This investigation examines the mono- Z' topology in the muonic decay channel of the neutral heavy gauge boson Z' . Monte Carlo simulation replicates proton-proton

* Ali.Hamed@bue.edu.eg

collisions at $\sqrt{s} = 14$ TeV with a substantial integrated luminosity of 1000 fb^{-1} at the LHC. This particular range of integrated luminosity at the LHC is called the High-Luminosity Large Hadron Collider (HL-LHC), the upcoming LHC upgrade expected to commence in 2028 [29]. The EFT scenario is the focal point of this study.

The paper is structured as follows: Section II briefly explains the EFT scenario in the context of mono- Z' portal. Section III briefly introduces the upcoming upgrade of the LHC, known as the HL-LHC, and the Compact Muon Solenoid (CMS) detector. Moving on to the methodology discussion, the simulated signal samples and their SM background sources are discussed in section IV. Following that, in section V, the event selection and the analysis approach are covered. The yielded results and conclusion of the study are presented in section VI and section VII, respectively.

II. THE EFT SCENARIO IN THE CONTEXT OF THE MONO- Z' PORTAL

The new DM model proposed in [19] suggests that DM production accompanied by a resonance yielded from a new neutral heavy gauge boson called the Z' is possible. This model comes in three different scenarios: the light vector (LV) scenario, referred to as the dark fermion scenario, the dark Higgs (DH) scenario, and the light vector accompanied by the coupling of inelastic effective field theory (EFT) scenario.

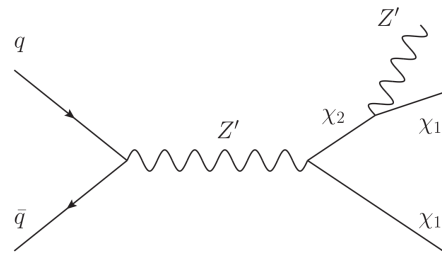
Scenario	Masses assumptions
Heavy dark sector	$M_{\chi_1} = M_{Z'}/2$ $M_{\chi_2} = 2M_{Z'}$

Table I The heavy dark sector mass assumptions for EFT scenario [19].

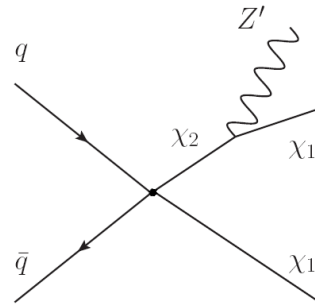
The EFT scenario differs from the LV scenario in that the DM and SM particle interactions are reduced to a contact interaction expressed in the Lagrangian interaction term shown in equation (1).

$$\frac{1}{2\Lambda^2} \bar{q} \gamma^\mu q (\bar{\chi}_2 \gamma^\mu \gamma^5 \chi_1 + \bar{\chi}_1 \gamma^\mu \gamma^5 \chi_2). \quad (1)$$

Figure 1 displays the Feynman diagram for the light vector (LV) 2(a) and the effective field theory (EFT) 2(b) scenario as taken from [19], while table I points to the dark sector mass assumption used for the process. The primary reason for opting for the EFT scenario instead of relying on extrapolated results from the LV scenario lies in the EFT's significantly longer tail in the MET distribution as explained in [19]. This distinctive feature allows it to stand out from the SM background more effectively. Additionally, we aim to establish a limit on



(a) The light vector (LV) diagram



(b) The effective field theory (EFT) diagram

Figure 1 The Feynman diagram for the light vector 2(a) and the effective field theory (EFT) 2(b) scenario as taken from [19].

the EFT cut-off scale (Λ), a parameter that has not been previously explored.

Throughout this paper, the SM leptons coupling with Z' is denoted as g_l , and the DM particles coupling with the Z' is denoted as g_D . The main free parameters of the EFT scenario are the model cut-off scale (Λ) and the Z' mass ($M_{Z'}$). Despite finding that changing g_l changes the corresponding cross-section values, g_l is chosen to be 0.1 to be consistent with the results of the ATLAS collaboration presented in [27].

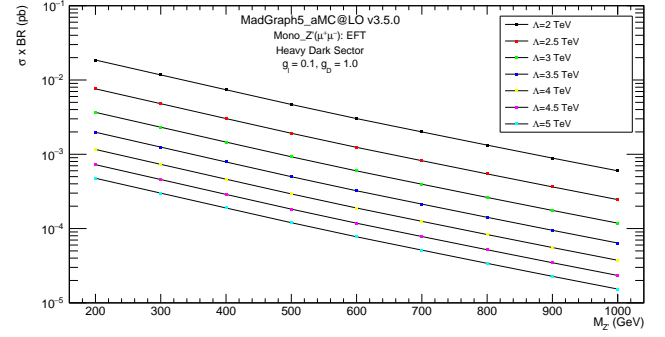
The study scope is on the Z' decay to dimuon $Z' \rightarrow \mu\bar{\mu}$ by simulating the behavior of the CMS detector. This choice was motivated by the CMS detector's optimization for detecting the muonic decay channel of $Z' \rightarrow \mu\bar{\mu}$. Additionally, we examined the range of masses in the heavy dark sector, as detailed in table I.

The EFT signal events of the model were generated using the general-purpose matrix element event generator known as MadGraph5_aMC@NLO v3.5.0 [30], at $\sqrt{s} = 14$ TeV. Table II lists the measurements of the cross-sections and the branching ratio product for various values of Λ and $M_{Z'}$. These generated data are used to set limits to the free parameters, Λ and $M_{Z'}$, as explained later in the results section.

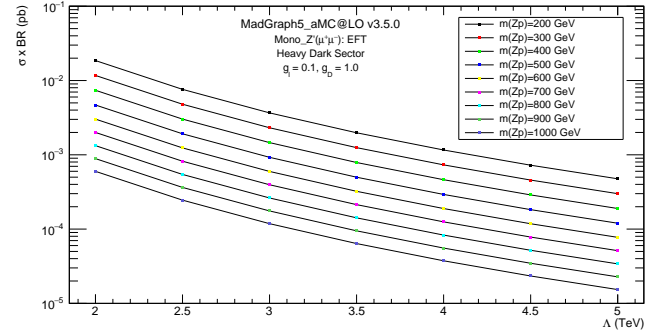
Figure 2 presents the production of the EFT signal cross-section versus $M_{Z'}$ 2(a) and Λ 2(b) at $\sqrt{s} = 14$ TeV. The cross-section times the branching ratio ($\sigma \times Br(Z' \rightarrow \mu\mu)$) is expected to decrease with Λ and $M_{Z'}$.

$M_{Z'}/(\text{GeV})$	200	300	400	500	600	700	800	900	1000	1500	2000
$\Lambda_{(\text{TeV})}$											
2	1.86×10^{-02}	1.17×10^{-02}	7.39×10^{-03}	4.68×10^{-03}	3.02×10^{-03}	2×10^{-03}	1.33×10^{-03}	8.88×10^{-04}	5.99×10^{-04}	8.173×10^{-05}	1.061×10^{-05}
2.5	7.61×10^{-03}	4.8×10^{-03}	3.03×10^{-03}	1.92×10^{-03}	1.24×10^{-03}	8.2×10^{-04}	5.44×10^{-04}	6.64×10^{-04}	2.45×10^{-04}	3.352×10^{-05}	4.344×10^{-06}
3	3.67×10^{-03}	2.31×10^{-03}	1.46×10^{-03}	9.25×10^{-04}	5.97×10^{-04}	3.95×10^{-04}	2.62×10^{-04}	1.76×10^{-04}	1.18×10^{-04}	1.617×10^{-05}	2.095×10^{-06}
3.5	1.98×10^{-03}	1.25×10^{-03}	7.88×10^{-04}	4.99×10^{-04}	3.23×10^{-04}	2.13×10^{-04}	1.42×10^{-04}	9.47×10^{-05}	6.39×10^{-05}	8.724×10^{-06}	1.131×10^{-06}
4	1.16×10^{-03}	7.32×10^{-04}	4.62×10^{-04}	2.93×10^{-04}	1.89×10^{-04}	1.25×10^{-04}	8.3×10^{-05}	5.55×10^{-05}	3.74×10^{-05}	5.128×10^{-06}	6.638×10^{-07}
4.5	7.25×10^{-04}	4.57×10^{-04}	2.88×10^{-04}	1.83×10^{-04}	1.18×10^{-04}	7.81×10^{-05}	5.18×10^{-05}	3.47×10^{-05}	2.34×10^{-05}	3.206×10^{-06}	4.149×10^{-07}
5	4.75×10^{-04}	3×10^{-04}	1.89×10^{-04}	1.2×10^{-04}	7.74×10^{-05}	5.12×10^{-05}	3.4×10^{-05}	2.27×10^{-05}	1.53×10^{-05}	2.091×10^{-06}	2.716×10^{-07}
10	2.971×10^{-05}	1.874×10^{-05}	1.183×10^{-05}	7.493×10^{-06}	4.838×10^{-06}	3.202×10^{-06}	2.126×10^{-06}	1.421×10^{-06}	9.583×10^{-07}	1.307×10^{-07}	1.702×10^{-08}
13	1.04×10^{-05}	6.561×10^{-06}	4.139×10^{-06}	2.624×10^{-06}	1.694×10^{-06}	1.121×10^{-06}	7.443×10^{-07}	4.997×10^{-07}	3.355×10^{-07}	4.576×10^{-08}	5.958×10^{-09}
Light vector	2.66×10^{-03}	5.03×10^{-04}	1.25×10^{-04}	4.08×10^{-05}	1.57×10^{-05}	6.64×10^{-06}	2.99×10^{-06}	1.42×10^{-06}	7.06×10^{-07}	2.90×10^{-08}	1.57×10^{-09}

Table II The readings of product of the EFT cross-section and branching ratio measured in (pb) and for the light vector scenario in the last row in the table for various values of $M_{Z'}$ and Λ in GeV and TeV, respectively, in the heavy dark sector, using the coupling constants values $g_D = 1.0$, $g_l = 0.1$, at $\sqrt{s} = 14$ TeV.



(a) $\sigma \times Br(Z' \rightarrow \mu\mu)$ vs $M_{Z'}$



(b) $\sigma \times Br(Z' \rightarrow \mu\mu)$ vs Λ

Figure 2 The plots of $\sigma \times Br(Z' \rightarrow \mu\mu)$ for the EFT signal versus $M_{Z'}$, 2(a), and Λ 2(b) regarding the scenario of EFT at $\sqrt{s} = 14$ TeV evaluated using MadGraph5.

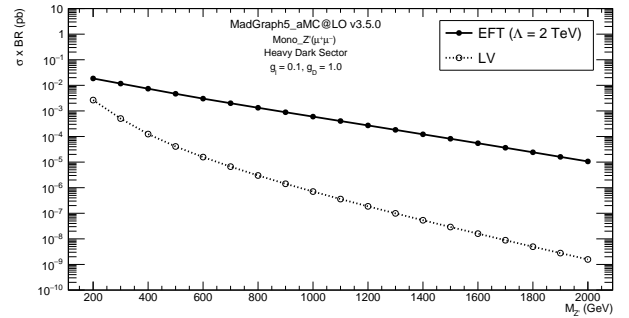


Figure 3 The curves of $\sigma \times Br(Z' \rightarrow \mu\mu)$ versus $M_{Z'}$, plotted for the EFT (closed circles) and LV (open circles) scenarios using the coupling constants values $g_D = 1.0$, $g_l = 0.1$, at $\sqrt{s} = 14$ TeV.

In Figure 3, we present the plots of $\sigma \times Br(Z' \rightarrow \mu\mu)$ against $M_{Z'}$, for both the effective field theory (EFT) and light vector (LV) scenarios. The data points for the EFT scenario are represented by closed circles corresponding to $\Lambda = 2$ TeV, while the LV scenario is shown with open circles. The coupling constants used in these calculations

are set to $g_D = 1.0$ and $g_l = 0.1$, with the center-of-mass energy fixed at $\sqrt{s} = 14$ TeV. The behavior of the EFT curve is considerably higher than the LV scenario, showing an increase of about one order of magnitude at low Z' mass and four orders of magnitude at high Z' mass.

III. THE HL-LHC PROJECT

Several upgrades have been conducted to the LHC, including Run I, Run II, and Run III, making it a worthy investment. The next upgrade, the HL-LHC, will increase the energy and the number of collisions, producing more data for statistical studies and accuracy. This upgrade requires new equipment to be installed over 1.2 km of the 27 km long LHC [29].

The CMS detector, a primary detector at CERN's LHC, aims to search for new physics using its complex structure. It employs different angular coordinates in its measurements, including the polar angle (θ), the azimuthal angle (ϕ), and the pseudo-rapidity (η).

The CMS detector coordinate system is as follows: the z-axis runs along the beam axis of the colliding particles, the x-axis is directed toward the LHC center, and the y-axis is directed upwards. The measurement of ϕ is in the x-y transverse plane, while θ is along the x-axis. Nevertheless, the direction of the colliding particles' products regarding the collision spot is described using η , defined as $\eta = -\ln[\tan(\theta/2)]$ [31–33].

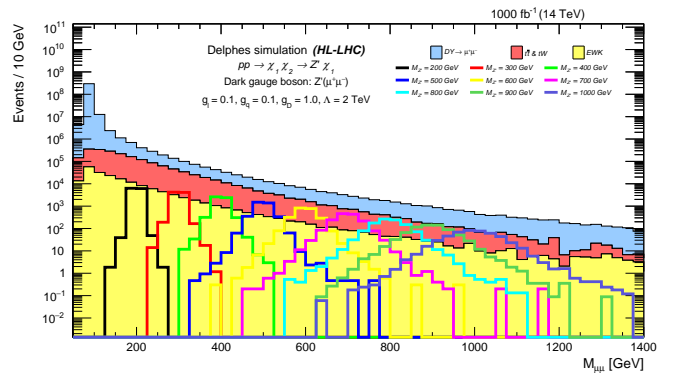
IV. MONTE CARLO SAMPLES SIMULATION

A. The Signal Samples Simulations

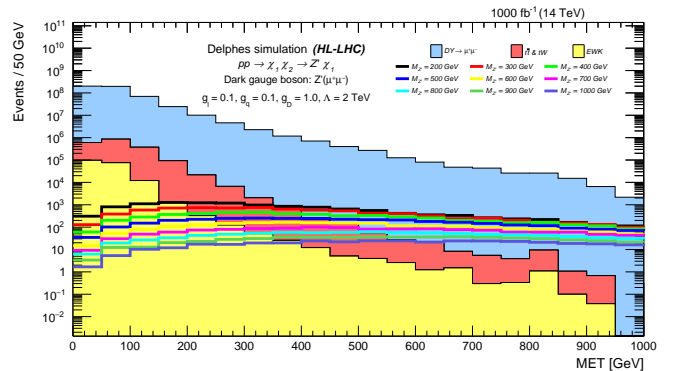
The signal events of the model were generated using MadGraph5_aMC@NLO v3.5.0 [30]. The next-to-leading-order (NLO) is used in cross-section calculations at $\sqrt{s} = 14$ TeV, and Pythia8 [34] is used for hadronization and parton showering processes. For fast detector simulation for CMS experiment, DELPHES [35] has been used. The EFT production cross-section calculations have been scanned for an extensive variety of the $M_{Z'}$, ranging from 200 GeV to 2000 GeV, and for Λ from 1 TeV to 5 TeV assuming the coupling constants values to be $g_l = 0.1$, and $g_D = 1.0$ as those used in [27, 28].

B. The Simulation of SM Backgrounds

In this analysis, the studied EFT signal topology is dimuon plus missing transverse energy ($\mu^+\mu^- + E_T^{miss}$). Therefore, several SM processes could mimic this topology via having muons and/or E_T^{miss} , arising from undetected neutrinos, in their final states. Such interactions are considered SM backgrounds for the signal. Those SM backgrounds are The Drell-Yan (DY) process ($DY \rightarrow \mu^+\mu^-$), the fully leptonic decay of top-quark pairs



(a) Dimuon invariant mass



(b) Missing transverse energy (E_T^{miss})

Figure 4 The histograms of the dimuon invariant mass 4(a), and the missing transverse energy 4(b) distributions regarding the expected SM background and the EFT scenario signal of different $M_{Z'}$ values in the heavy-dark sector at $\Lambda = 2$ TeV after applying the preliminary selection, listed in table III.

($t\bar{t} \rightarrow \mu^+\mu^- + 2b + 2\nu$), the single top process ($t\bar{t}W^+ \rightarrow \mu^+\mu^- + 2b + 2\nu$, $tW^- \rightarrow \mu^+\mu^- + 2b + 2\nu$), and the electroweak diboson channels production ($W^+W^- \rightarrow \mu^+\mu^- + 2\nu$, $W^\pm Z \rightarrow \mu^\pm\mu^+\mu^- + \nu$, $ZZ \rightarrow \mu^+\mu^- + 2\nu$, and $ZZ \rightarrow \mu^+\mu^-\mu^+\mu^-$). All these Monte Carlo Samples have a cross-section calculated at NLO using MadGraph5_aMC@NLO v3.5.0 [30] interfaced with Pythia8 [34] for hadronization and modeling. All contributions of SM background processes and signal samples are estimated using Monte Carlo Simulation and normalized to their corresponding cross-section with 1000 fb^{-1} integrated luminosity.

V. SELECTION OF EVENTS

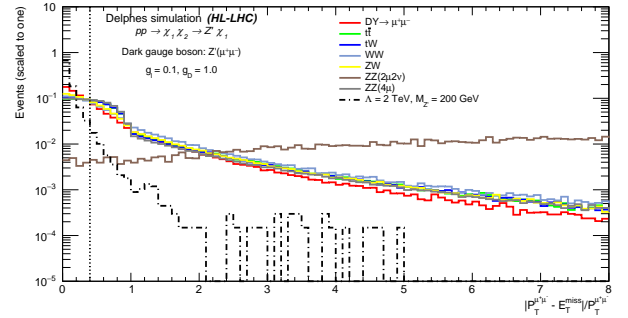
In this analysis, the event selection is designed to reconstruct two-high- p_T muons of opposite charges associated with E_T^{miss} , referring to DM candidates, in the final state. This selection is presented as applied cuts to different kinematics requiring muons to pass the preliminary selection shown in table III.

Thus, each muon should be with $p_T^\mu > 30$ GeV and $|\eta^\mu| < 2.4$, in addition, this muon must be isolated and pass the following criteria "IsolationVarRhoCorr" referring to the isolation cut in DELPHES to eliminate muons produced inside jets. For this cut, corrected for the pileup effect, the scalar summation of the p_T of all the tracks of muons should not go beyond 10% of the muon p_T^μ . This must be in the limits of a $\Delta R = 0.5$ cone surrounding the muon candidate, except the candidate itself. The dimuon invariant mass is greater than 60 GeV as we search for a high mass regime resonance.

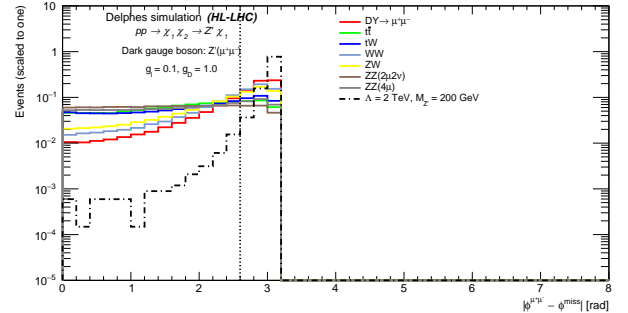
Figure 4(a) displays the histograms of the dimuon invariant mass distribution for the signal and the stacked background histograms. The blue histogram, the dominant background, refers to the DY background, while the yellow one is for the electroweak background of vector boson pairs (ZZ, WW, and WZ). The backgrounds of the top-quark pair ($t\bar{t}$), and the single top (tW) are denoted by the red histogram. The different colored lines overlaid on the stacked histograms of the background represent the EFT signal, generated for various values of the $M_{Z'}$, in the heavy-dark sector masses assumptions, and a fixed value of $\Lambda = 2$ TeV. The corresponding E_T^{miss} distribution is illustrated in figure 4(b).

In figures 4(a) and 4(b), as the background overwhelms the signal, we need a tighter set of discrimination cuts to distinguish between the signals and the SM backgrounds. We have four-cut parameters: the first one is the requirement of the dimuon invariant mass to be restricted to a small range of the $M_{Z'}$, where $0.9 \times M_{Z'} < M_{\mu^+\mu^-} < M_{Z'} + 25$ as recommended by [19]. Secondly is the selection of the relative difference of the dimuon transverse momentum ($P_T^{\mu^+\mu^-}$) and the E_T^{miss} to be less than 0.4 (i.e. $|P_T^{\mu^+\mu^-} - E_T^{miss}| / P_T^{\mu^+\mu^-} < 0.4$). The third parameter is the cone radius $\Delta R(\mu^+\mu^-)$ to be less than 3.2 (i.e. $\Delta R(\mu^+\mu^-) < 3.2$). The fourth and last parameter is the azimuthal angle between the dimuon and the E_T^{miss} directions, defined as $\Delta\Phi_{\mu^+\mu^-, E_T^{miss}} = |\Phi^{\mu^+\mu^-} - \Phi^{miss}|$, to be selected as $\Delta\Phi_{\mu^+\mu^-, E_T^{miss}} > 2.6$. Table III summarizes these selection criteria.

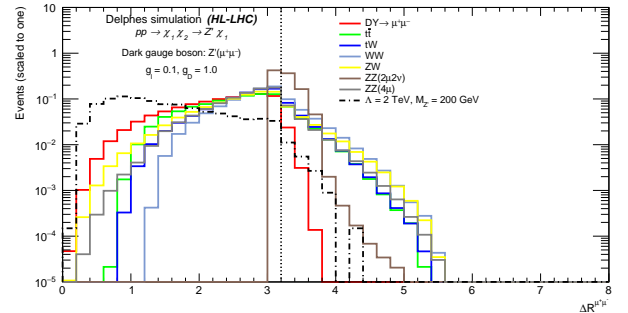
Figure 5 shows the distributions, scaled to one, of $|P_T^{\mu^+\mu^-} - E_T^{miss}| / P_T^{\mu^+\mu^-}$ 5(a), $\Delta\Phi_{\mu^+\mu^-, E_T^{miss}}$ 5(b), and $\Delta R(\mu^+\mu^-)$ 5(c) with their corresponding cutting values for dimuons events applied to the SM background and the generated signal of the EFT scenario in the heavy dark sector for $M_{Z'} = 200$ GeV and $\Lambda = 2$ TeV. The application of the mass window cut ($0.9 \times M_{Z'} < M_{\mu^+\mu^-} < M_{Z'} + 25$) fully suppresses the $ZZ \rightarrow \mu^+\mu^- + 2\nu$ background. The next section presents the results of applying these cuts to the E_T^{miss} showing how strongly these cuts reduced the SM background for the sake of discrimination between the signal and the SM background.



(a) $|P_T^{\mu^+\mu^-} - E_T^{miss}| / P_T^{\mu^+\mu^-}$



(b) $\Delta\Phi_{\mu^+\mu^-, E_T^{miss}}$



(c) $\Delta R(\mu^+\mu^-)$

Figure 5 The histograms correspond to the EFT scenario signal ($\Lambda = 2$ TeV, and $M_{Z'} = 200$ GeV), and SM backgrounds. The histograms are normalized to unity to highlight qualitative features, and the vertical dashed lines correspond to the chosen cut value per each variable.

VI. RESULTS

The shape-based analysis is chosen based on the E_T^{miss} distribution because of the good discrimination it gives between the model's signal and the SM background combination. Figure 6 displays the invariant mass distribution of the dimuon pairs, related to the production of Z' , after applying the preliminary and tight cuts, listed in

Step	Criteria	Requirements
Preliminary selection	p_T^μ (GeV)	> 30
	$ \eta^\mu $ (rad)	< 2.4
	IsolationVarRhoCorr	< 0.1
	$M_{\mu^+\mu^-}$ (GeV)	> 60
Tight selection	$\Delta R(\mu^+\mu^-)$	< 3.2
	$\Delta\phi_{\mu^+\mu^-}, \vec{E}_T^{miss}$	> 2.6
	$ P_T^{\mu^+\mu^-} - E_T^{miss} /P_T^{\mu^+\mu^-}$	< 0.4
	Mass window (GeV)	$0.9 \times M_{Z'} < M_{\mu^+\mu^-} < M_{Z'} + 25$

Table III Summary of the preliminary and tight cuts of the final event selection used in this cut-based analysis.

table III, except the mass window cut. As noticed, there is a significant decrease in the SM backgrounds while preserving the signal strength, as demonstrated by the comparison of figures 4(a) and 6 for the EFT scenario. Figure 7 illustrates the E_T^{miss} distribution after applying the all cuts presented in table III.

This analysis also introduces a calculation of the signal statistical significance (S) over the SM backgrounds using the Asimov formula, equation (2), described in [36].

$$S = \sqrt{2 \times \left((N_s + N_b) \log\left(1 + \frac{N_s}{N_b}\right) - N_s \right)}, \quad (2)$$

where N_s and N_b are the number of events of the signal and the total SM backgrounds, respectively, passing the final selections shown in table III. This investigation assessed the significance at the five sigma level (5σ) with high integrated luminosity values for the EFT scenario at $\sqrt{s} = 14$ TeV. We explored different values of Λ while keeping $M_{Z'}$ fixed at 600 GeV in 8(a), and we also examined various values of $M_{Z'}$ with Λ fixed at 4 TeV in 8(b). Our findings revealed that a 5σ significance can be achieved at an integrated luminosity of about 1900 fb^{-1} for $M_{Z'} = 600$ GeV and $\Lambda = 4$ TeV, as illustrated in figure 8(b).

We utilized the profile likelihood method to statistically analyze our findings and conducted a statistical test. Employing the modified frequentist construction CLs [37, 38], which is grounded on the asymptotic approximation [36], we determined exclusion limits on the product of signal cross sections and the branching fraction $\text{Br}(Z' \rightarrow \mu\mu)$ at a 95% confidence level.

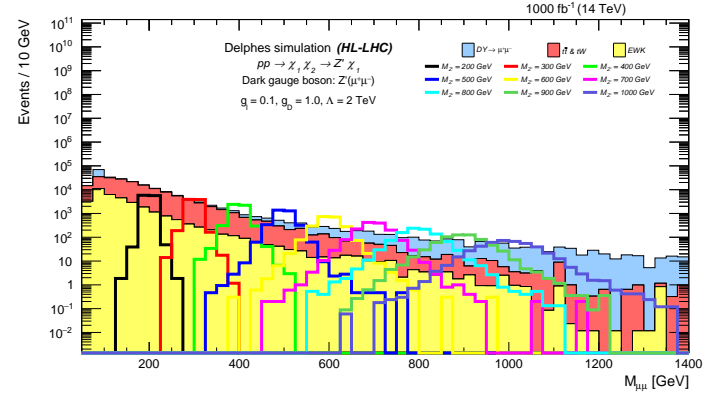


Figure 6 The histograms of dimuon invariant mass for the anticipated SM backgrounds and the generated signal of the EFT scenario for $M_{Z'} = 200$ GeV in the heavy-dark sector at $\Lambda = 2$ TeV after applying all cuts, listed in table III, except the mass window cut

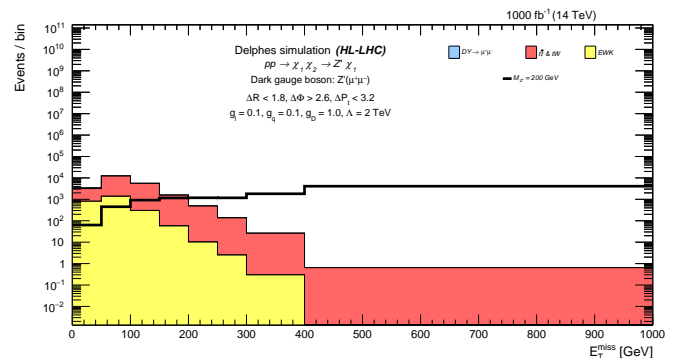


Figure 7 The histograms of the missing transverse energy regarding the anticipated SM background and the generated signal of the EFT scenario for $M_{Z'} = 200$ GeV in the heavy-dark sector at $\Lambda = 2$ TeV after applying all cuts, listed in table III.

In Figure 9 illustrates the 95% upper limit on $\sigma \times \text{Br}(Z' \rightarrow \mu\mu)$ plotted against $M_{Z'}$ for the EFT scenario based on the mono- Z' portal. This specifically pertains to the muonic decay of Z' and the values of the coupling constants ($g_D = 1.0$, $g_l = 0.1$) in the heavy dark sector,

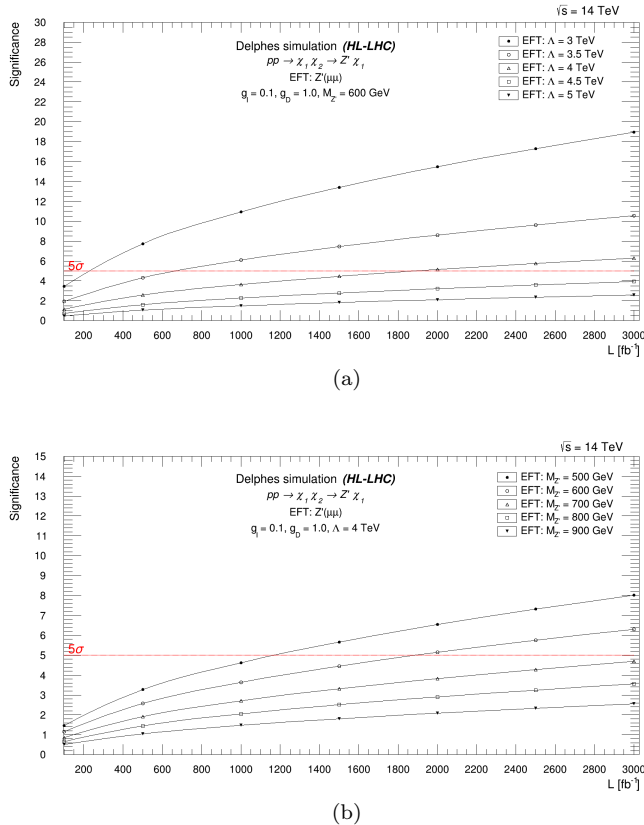


Figure 8 The five sigma significance of the EFT scenario versus the HL-LHC integrated luminosity plotted for different values of Λ at $M_{Z'} = 600$ GeV in 8(a), and for several values of $M_{Z'}$ at $\Lambda = 4$ TeV in 8(b).

as detailed in table I, for various Λ values. The solid curves in this plot represent the theoretical $\sigma \times Br(Z' \rightarrow \mu\mu)$ corresponding to the EFT scenario for specific values of Λ . Based on figure 9, the production of the Z' is ruled out in the mass range of 200 to 1929 GeV for $\Lambda = 2$ TeV, and from 200 to 1305 GeV for $\Lambda = 4$ TeV as indicated from the expected median. Above $\Lambda = 13$ TeV the LHC is not sensitive to this EFT model.

Figure 10 presents the anticipated exclusion limits at a 95% CL resulting from the EFT scenario search with 1000 fb^{-1} of 14 TeV proton-proton collision simulated data. These limits are presented as a function of $M_{Z'}$ and Λ . The colored region represents the upper limit, while a dashed black line denotes the median of the expected limits.

VII. SUMMARY

This study proposed a search for a Z' boson decaying into dimuon in association with neutral particles (DM particles χ_1 and χ_2) in the framework of the EFT scenario.

Monte Carlo simulations of proton-proton collisions at $\sqrt{s} = 14$ TeV for 1000 fb^{-1} integrated luminosity, corresponding to the HL-LHC project were used. The analysis presented results of the muonic decay of Z' for the heavy dark sector ($M_{\chi_1} = M_{Z'}/2$, and $M_{\chi_2} = 2M_{Z'}$), given that the coupling constants are fixed and chosen to be $g_l = 0.1$ and $g_D = 1.0$. 95% CL limit on the model's free parameters is shown for Λ and $M_{Z'}$.

Based on the analysis final event selection outlined in table III, it is feasible to achieve a 5σ discovery of the Z' heavy gauge boson in the $\mu^+\mu^-$ decay channel. This is achievable for Z' mass values ranging from 500 to 600 GeV, with Λ set at 4 TeV. To do this, an integrated luminosity of less than 1900 fb^{-1} is required at the 14 TeV center of mass energy of the HL-LHC. However, Z' mass exceeding 600 GeV cannot be detected.

A previous study by the ATLAS collaboration [27], has used the full run-2 data taken by the LHC at $\sqrt{s} = 13$ TeV of proton-proton collisions with an integrated luminosity of 14 fb^{-1} . Which has excluded Z' masses ranging from 200 to 450 GeV within the heavy dark sector of the LV scenario for $g_q = g_l = 0.1$ and $g_D = 1.0$.

If the signal is not detected at the HL-LHC with a center of mass energy of 14 TeV, we establish upper limits on the mass of Z' and the effective field theory (EFT) cut-off scale (Λ) at the 95% confidence level for the charged muonic decay channel of Z' . Specifically, limits have been determined for the EFT scenario with $g_q = g_l = 0.1$ and $g_D = 1.0$, ruling out the invariant mass range from 200 to 1929 GeV for $\Lambda \in [2, 13]$ TeV, while notably excluding $\Lambda = 13$ TeV at $M_{Z'} = 201.5$ GeV. Furthermore, for exceedingly high values of the EFT cut-off scale (i.e., $\Lambda > 13$ TeV), the HL-LHC will lack sensitivity to the EFT scenario.

Our upper limits on the signal process cross-section, when compared to the results from the ATLAS study in [27] at $\sqrt{s} = 13$ TeV, clearly show that our findings exceed those from the dimuon channel in the LV model scenario by more than an order of magnitude. This discrepancy can be attributed to the behavior of the cross-section for the effective field theory (EFT) curve, which is significantly higher than in the LV scenario. Specifically, we observe an increase of about one order of magnitude at low Z' masses and four orders of magnitude at high Z' masses. This substantial difference helps explain the main reason behind our improved results.

VIII. ACKNOWLEDGMENTS

The author of this paper appreciates the help of Tongyan Lin, an author in [19], for sending us the Universal FeynRules Output (UFO) file for the model used in the generation of the events. We also want to thank Mahmoud Hashim for his help with the IT issues faced throughout this work.

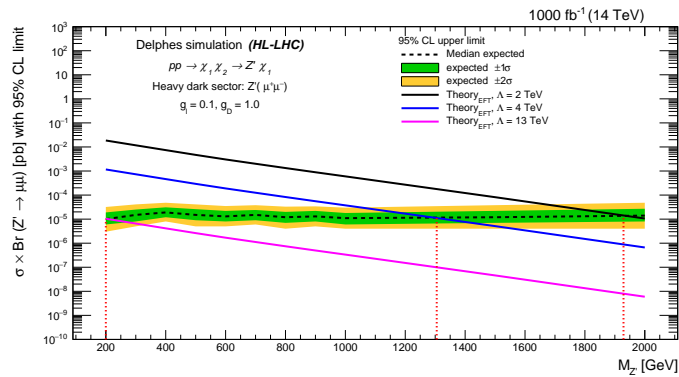


Figure 9 95% CL upper limits on the $\sigma \times Br(Z' \rightarrow \mu\mu)$ (expected), as a function of the Z' mass based on Mono- Z' model, with the muonic decay of the Z' . The solid lines represent the EFT scenario with different cut-off scales $\Lambda = 2$ TeV (in black), 4 TeV (in blue), and 13 TeV (in pink). The vertical dotted red lines indicate the upper limit values.

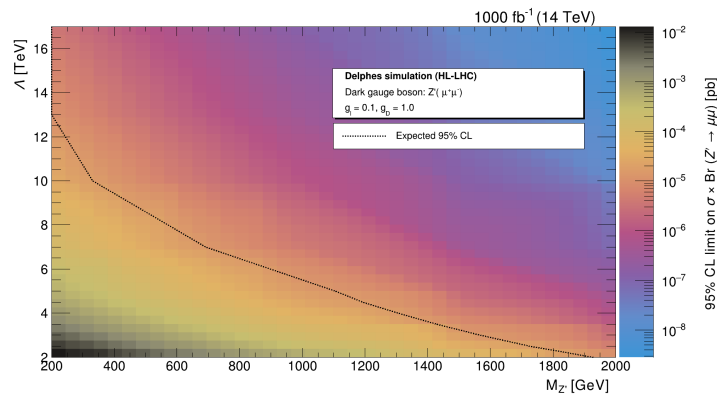


Figure 10 The upper limits at a 95% CL on $\sigma \times Br(Z' \rightarrow \mu\mu)$ are determined from the inclusive search, considering different pairs of EFT scenario parameters (Λ and $M_{Z'}$). The colored region represents the upper limit, while the dashed black line shows the expected exclusions for the nominal Z' cross-section.

-
- [1] F. Zwicky, *Helv. Phys. Acta* **6** (1933) 110.
- [2] R. J. Scherrer and M. S. Turner, On the relic, cosmic abundance of stable, weakly interacting massive. *Phys. Rev. D* **33** (1986) 1585.
- [3] P. A. R. Ade et al., Planck 2015 results. XIII. Cosmological parameters. *Astron. Astrophys.* **594** (2016) A13.
- [4] Y. Sofue and V. Rubin, Rotation Curves of Spiral Galaxies. *Annu. Rev. Astron. Astrophys.* **39** (2001) 137.
- [5] V. Trimble, Existence and Nature of Dark Matter in the Universe. *Annu. Rev. Astron. Astrophys.* **25** (1987) 425.
- [6] G. Bertone, D. Hooper, and J. Silk, Particle Dark Matter: Evidence, Candidates and Constraints. *Phys. Rept.* **405:279-390**, 2005.
- [7] L. Bergström, Non-Baryonic Dark Matter - Observational Evidence and Detection Methods. *Rept. Prog. Phys.* **63:793**, 2000.
- [8] K. Abazajian, G. M. Fuller, and M. Patel, Sterile neutrino hot, warm, and cold dark matter. *Phys. Rev. D* **64** (2001) 023501.
- [9] C. Lage and G. R. Farrar, The bullet cluster is not a cosmological anomaly. *J. Cosmol. Astropart. Phys.* **2015** (2015) 038.
- [10] G. Ross, *Nature* **311** (1984) 5986.
- [11] CMS Collaboration, Observation of a new boson at a mass of 125 GeV with the CMS experiment at the LHC. *Phys. Lett. B* **716** (2012) 30.
- [12] P. Langacker, *The Standard Model and Beyond*, Taylor & Francis, 2017.
- [13] CMS Collaboration, Search for new particles in events with energetic jets and large missing transverse momentum in proton-proton collisions at $\sqrt{s} = 13$ TeV. *JHEP* **11** (2021) 153.
- [14] CMS Collaboration, Search for dark matter produced in association with a leptonically decaying Z boson in proton-proton collisions at $\sqrt{s} = 13$ TeV. *Eur. Phys. J. C* **81** (2021) 13; Erratum: *Eur. Phys. J. C* **81** (2021) 333.
- [15] CMS Collaboration, Search for invisible decays of the Higgs boson produced via vector boson fusion in proton-proton collisions at $\sqrt{s} = 13$ TeV. *Phys. Rev. D* **105**

- (2022) 092007.
- [16] CMS Collaboration, Search for dark matter produced in association with a Higgs boson decaying to a pair of bottom quarks in proton-proton collisions at $\sqrt{s} = 13$ TeV. *Eur. Phys. J. C* **79** (2019) 280.
- [17] CMS Collaboration, Search for new physics in final states with a single photon and missing transverse momentum in proton-proton collisions at $\sqrt{s} = 13$ TeV. *JHEP* **02** (2019) 074.
- [18] CMS Collaboration, Search for dark matter produced in association with a single top quark or a top quark pair in proton-proton collisions at $\sqrt{s} = 13$ TeV. *JHEP* **03** (2019) 141.
- [19] M. Autran et al., Searches for dark matter in events with a resonance and missing transverse energy. *Phys. Rev. D* **92** (2015) 035007.
- [20] Y. Bai, J. Bourbeau, and T. Lin, Dark matter searches with a mono- Z' jet. *JHEP* **06** (2015) 205.
- [21] M. Cvetič and S. Godfrey, “Discovery and identification of extra gauge bosons”, [arXiv:hep-ph/9504216](https://arxiv.org/abs/hep-ph/9504216).
- [22] A. Leike, “The Phenomenology of extra neutral gauge bosons”, *Phy. Rep.* **317**, 143 (1999) [[arXiv:hep-ph/9805494](https://arxiv.org/abs/hep-ph/9805494)].
- [23] M. Cvetič, P. Langacker, and B. Kayser, “Determination of g-R / g-L in left-right symmetric models at hadron colliders”, *Phys. Rev. Lett.* **68** (1992) 2871.
- [24] S. Dimopoulos and H. Georgi, “Softly Broken Supersymmetry And SU(5)”, *Nucl. Phys. B* **193** (1981) 150.
- [25] CMS Collaboration, Search for resonant and nonresonant new phenomena in high-mass dilepton final state at $\sqrt{s} = 13$ TeV, *JHEP* **07** (2021) 208 [[arXiv:2103.02708v2](https://arxiv.org/abs/2103.02708v2)] [[hep-ex](#)].
- [26] ATLAS Collaboration, Search for high-mass dilepton resonances using 139 fb^{-1} of pp collision data collected at $\sqrt{s} = 13$ TeV with the ATLAS detector, *Phys. Lett. B* **796** (2019) 68.
- [27] ATLAS Collaboration, Search for a new leptonically decaying neutral vector boson in association with missing transverse energy in proton-proton collisions at $\sqrt{s} = 13$ TeV with the ATLAS detector, ATLAS-CONF-2023-045 (2023).
- [28] ATLAS Collaboration, Search for dark matter in events with a hadronically decaying vector boson and missing transverse momentum in pp collisions at $\sqrt{s} = 13$ TeV with the ATLAS detector. *JHEP* **10** (2018) 180.
- [29] O. Brüning and L. Rossi, in *The High Luminosity Large Hadron Collider: New Machine for Illuminating the Mysteries of the Universe*, edited by T. Dumont and L. Rossi (2024), pp. 1-53.
- [30] J. Alwall et al., *J. High Energy Phys.* **2014** (2014) 07.
- [31] G. Grégoire et al., *J. Instrum.* **3** (2008) S08004.
- [32] CMS Collaboration, *J. Instrum.* **3** (2008) S08004.
- [33] G. L. Bayatian, *J. Phys. G* **34** (2007) CERN-LHCC-2006-021; CMS-TDR-008-2; FERMILAB-CONF-07-831-CMS.
- [34] T. Sjöstrand, S. Mrenna, and P. Skands, *J. High Energy Phys.* **2006** (2006) 05.
- [35] J. de Favereau et al., *J. High Energy Phys.* **2014** (2014) 02.
- [36] G. Cowan et al., Asymptotic formulae for likelihood-based tests of new physics, *Eur. Phys. J. C* **71** (2011), p. 1554, doi: 10.1140/epjc/s10052-011-1554-0, [arXiv:1007.1727](https://arxiv.org/abs/1007.1727) [[physics.data-an](#)], Erratum: *Eur. Phys. J. C* **73** (2013) 2501.
- [37] A. L. Read, Presentation of search results: the CLs technique, *J. Phys. G: Nucl. Part. Phys.* **28** (2002) 2693, doi:10.1088/0954-3899/28/10/313.
- [38] T. Junk, Confidence level computation for combining searches with small statistics, *Nuclear Instruments and Methods in Physics Research Section A: Accelerators, Spectrometers, Detectors and Associated Equipment*, Volume 434, Issues 2–3, 1999, Pages 435-443, ISSN 0168-9002, [https://doi.org/10.1016/S0168-9002\(99\)00498-2](https://doi.org/10.1016/S0168-9002(99)00498-2).